ISSN 1063-7710, Acoustical Physics, 2012, Vol. 58, No. 6, pp. 642–649. © Pleiades Publishing, Ltd., 2012.

CLASSICAL PROBLEMS OF LINEAR ACOUSTICS AND WAVE THEORY

Diamond-Shaped Acoustic Concentrator with Homogeneous Material Parameters[1]

Tinghua Li, Ming Huang, Jingjing Yang, Yalin Li, and Jiang Yu

Wireless Innovation Lab, School of Information Science and Engineering, Yunnan University, Kunming, 650091 P.R. China

e-mail: huangming@ynu.edu.cn

Received January 10, 2012

Abstract—Based on coordinate transformation method, the two-dimensional and three-dimensional acoustic concentrators with diamond shape composed of nonsingular homogeneous materials are designed in this paper. The mass density tensor and bulk modulus of the acoustic concentrators are derived. Performance of the concentrators is confirmed by full-wave simulation. The work represents an important progress towards the practical realization of the metamaterial-assisted acoustic concentrator and expands the application of the coordinate transformation method.

Keywords: transformation acoustics, metamaterials, acoustic concentrator

DOI: 10.1134/S1063771012060085

1. INTRODUCTION

Since control of electromagnetic fields using the coordinate transformation method was generalized by Pendry and Leonhardt et al. [1, 2], more and more researches have been putting their efforts into this exciting topic [3–15]. Following this method, invisibility cloaks were soon confirmed by full-wave simulations [3] and experimentally realized at microwave and optical frequencies [4, 5] with the help of metamaterials. Some other interesting devices with novel functionalities have also been reported, such as field-rotating device [11], beam splitter [12] and field concentrator [13]. Inspired by these pioneering works, the coordinate transformation method is further extended to acoustic field and opens up many possibilities to control acoustic wave with unprecedented degrees of freedom. The most intriguing possibility is to design an acoustic cloak that can make a domain undetectable by acoustic waves [16–18]. Apart from the cloak, the method can lead to many novel wave manipulation strategies pretty much the same way it can do for electromagnetic waves. For example, Chen et al. [19] proposed a field rotator that can rotate the wave front of the linear liquid surface waves. Perfect acoustic imaging with complementary media is numerically demonstrated in two dimensions by Han et al. [20]. Yang et al. [21] investigated the two dimensional (2D) cylindrical acoustic superscatterer, and discussed its multilayer realization approach. Ren et al. [22] presented a four-beam acoustic antenna by merging the conformal mapping and the embedded coordinate transformation method. An acoustic planar hyperlens capable of magnifying sub-diffraction-limit objects on one flat surface and forming magnified images on another flat surface was designed by Wu et al. [23], and so on. A review of this large body of work has been provided by Chen et al. [24], and some interesting results about acoustic focusing have been reported [25, 26]. But to the best of our knowledge, there is no report about the acoustic concentrator, which plays an important role in harnessing of sound wave in underwater sonar or similar devices where high pressure field is required.

Recently, our Lab developed the material parameter expressions for acoustic metamaterial concentrators with arbitrary N-sided regular polygonal cross section, and this investigation has many potential applications in acoustic field [27]. Unfortunately, the practical fabrication of this concentrator has so far not been achievable, for the material parameters (i.e. mass density tensors and bulk modulus) are spatially inhomogeneous and even singular. To remove the two bottlenecks, we extend the 2D homogeneous-materials-constructed electromagnetic field concentrator proposed by Li et al. [28] to acoustic field. Moreover, to make the model more realistic, a three-step linear transformation method is proposed for designing three dimensional (3D) diamond-shaped acoustic concentrator composed of tetrahedral homogeneous blocks with finite values. Full wave simulations based on finite element method are performed to demonstrate the designed material parameters. We show that the proposed concentrator has good concentrating performance for all incident direction under plane wave and cylindrical wave irradiation, and its material parameters are nonsingular homogeneous. The work would

[1] The article is published in the original.

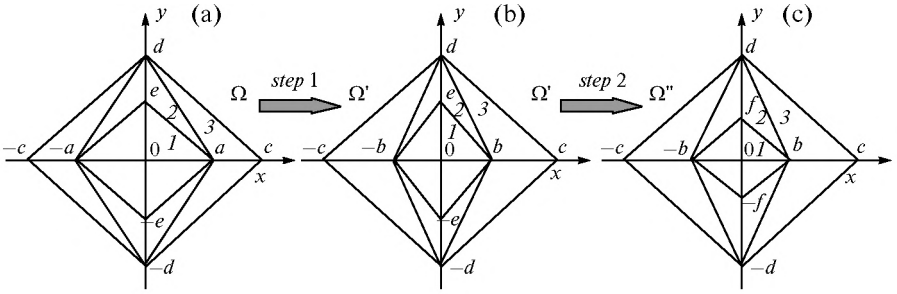

Fig. 1. Schematic diagram of the coordinate transformation for the design of 2D acoustic concentrator.

move the acoustic concentrator a step further towards the practical realization.

2. METHOD AND SIMULATION MODEL

According to the coordinate transformation method, under a space transformation from

the original coordinate (x_1, x_2, x_3) to a new coordinate $(x'_1(x_1, x_2, x_3), x'_2(x_1, x_2, x_3), x'_3(x_1, x_2, x_3))$, the mass density tensor ρ' and bulk modulus κ' in the transformed space can be written as [17]

$$\rho'^{-1} = A\rho^{-1}A^T/\det A, \quad \kappa' = \kappa \det A, \tag{1}$$

where ρ and κ are the mass density tensor and bulk modulus of the original space, A is the Jacobian transformation matrix with components $A_{ij} = \partial x'_i/\partial x_j$. It characterizes the mapping from the original space to the transformed space. det**A** is the determinant of the matrix. The determination of matrix **A** is the key issue for designing the transformation mediums.

2.1. 2D Acoustic Concentrator

Figure 1 shows a schematic diagram of the coordinate transformation for the design of 2D acoustic concentrator. The original space (x, y), the transitional space (x', y'), and the transformed space (x'', y'') are shown in Figs. 1a–1c, respectively. The transformation proceeds in two steps, i.e. *step* 1 and *step* 2. The *step* 1 is to compress line segment *2a* to *2b* in the x direction, while keep the y direction unchanged. The *step* 2 is to compress line segment *2e* to *2f* in y direction. Taking the space in the first quadrant as an example, in the original space, regions *1*, *2*, and *3* in Fig. 1a are composed of area *aoe, ade* and *acd*, respectively. After the *step* 1, the areas *aoe*, *ade* and *acd* are transformed into areas *boe*, *bde* and *bcd* in the transitional space, as shown in Fig. 1b. Thus, the regions *1* and *2* are compressed, while region *3* is relatively stretched. For each region, the coordinate transformation can be obtained as follows.

$$\text{Region 1: } x' = \frac{b}{a}x, \quad y' = y, \quad z' = z; \tag{2}$$

$$\text{Region 2: } x' = \frac{b}{a}x, \quad y' = y, \quad z' = z; \tag{3}$$

$$\text{Region 3: } x' = \frac{c-b}{c-a}x - \frac{c}{d}\frac{(a-b)}{(a-c)}y + \frac{c(a-b)}{a-c}, \quad y' = y, \quad z' = z. \tag{4}$$

In *step* 2, the transitional space is further mapped onto transformed space, as shown in Fig. 1c. Similar to *step* 1 in which distortion only happens in the x direction, the space is compressed or stretched only in the y direction in the *step* 2. After the transformation, area *boe* is compressed to area *bof* and area *bde* is stretched to area *bdf*, while area *bcd* experience no change. The corresponding coordinate transformation for each region can be expressed by the following equations.

$$\text{Region 1: } x'' = x', \quad y'' = \frac{f}{e}y', \quad z'' = z'; \tag{5}$$

$$\text{Region 2: } x'' = x', \quad y'' = -\frac{d(e-f)}{b(e-d)}x' + \frac{d-f}{d-e}y' + \frac{d(e-f)}{e-d}, \quad z'' = z'; \tag{6}$$

$$\text{Region 3: } x'' = x', \quad y' = y, \quad z' = z. \tag{7}$$

Combining the two steps, the final transformation equations can be obtained.

$$\text{Region 1: } x'' = \frac{b}{a}x, \quad y'' = \frac{e}{f}y, \quad z'' = z; \tag{8}$$

$$\text{Region 2: } x'' = \frac{b}{a}x, \quad y'' = -\frac{d(e-f)}{a(e-d)}x + \frac{d-f}{d-e}y + \frac{d(e-f)}{e-d}, \quad z'' = z'; \tag{9}$$

$$\text{Region 3: } x' = \frac{c-b}{c-a}x - \frac{c}{d}\frac{(a-b)}{(a-c)}y + \frac{c(a-b)}{a-c}, \quad y'' = y, \quad z'' = z. \tag{10}$$

According to (1), the relative mass density tensors and bulk modulus of 2D acoustic concentrator in the transformation regions *1*, *2*, and *3* can be expressed as

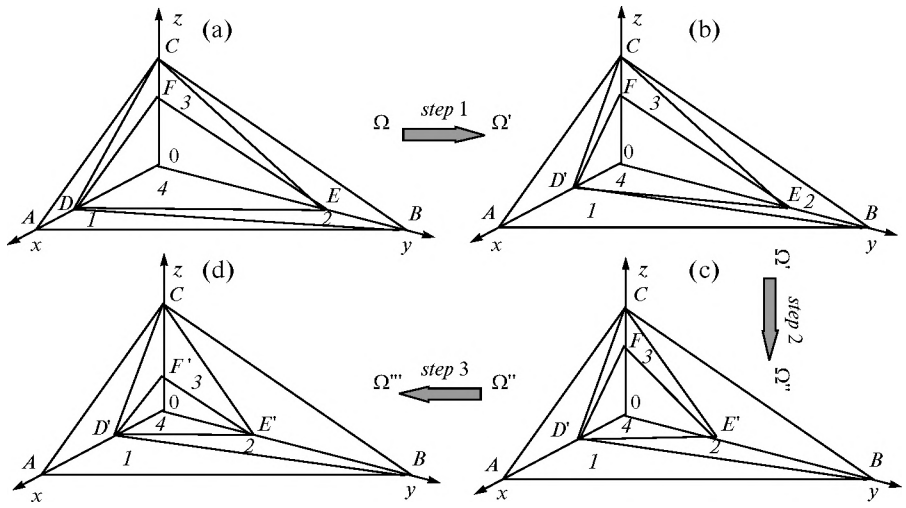

Fig. 2. Schematic diagram of the coordinate transformation for the design of 3D acoustic concentrator.

$$\text{Region 1: } \frac{1}{\rho_1'} = \begin{bmatrix} A/B & 0 & 0 \\ 0 & B/A & 0 \\ 0 & 0 & 1/(AB) \end{bmatrix} \frac{1}{\rho}, \quad (11)$$

$$\kappa' = AB\kappa;$$

$$\text{Region 2: } \frac{1}{\rho_2'}$$

$$= \begin{bmatrix} A/E & -CD/E & 0 \\ -CD/E & (C^2D^2 + E^2)/(AE) & 0 \\ 0 & 0 & 1/(AE) \end{bmatrix} \frac{1}{\rho}, \quad \kappa' = AE\kappa; \quad (12)$$

$$\text{Region 3: } \frac{1}{\rho_3'} = \begin{bmatrix} (F^2 + G^2H^2)/F & -GH/F & 0 \\ -GH/F & 1/F & 0 \\ 0 & 0 & 1/F \end{bmatrix} \frac{1}{\rho}, \quad (13)$$

$$\kappa' = F\kappa,$$

where $A = b/a$, $B = f/e$, $C = d/a$, $D = (e - f)/(e - d)$, $E = (d - f)/(d - e)$, $F = (c - b)/(c - a)$, $G = (a - b)/(a - c)$, $H = c/d$.

The mass density tensor and bulk modulus of 2D acoustic concentrator in the other quadrants can be calculated similarly. Obviously, the material parameters are spatially invariant once the geometry parameters have been fixed, and there is no singularity. These two features are valuable for the practical realization of the acoustic concentrator.

2.2. 3D Acoustic Concentrator

The 3D diamond-shaped acoustic concentrator is divided into eight parts by the x, y, z coordinate axes. The schematic diagram of the coordinate transformation for the design of the first part of the 3D concentrator in the first quadrant is shown in Fig. 2. The other parts are axially symmetrical to the first part, and it is not shown here for brevity. Figures 2a–2d show the original space (x, y, z), the transitional space (x', y', z'), (x'', y'', z''), and the transformed space (x''', y''', z'''), respectively. The 3D concentrator can be obtained through a three-step linear transformation. The first step (*step* 1) is to compress OD to OD' in the x-axis direction, while keep the y-axis and z-axis undistorted. The second step (*step* 2) is similar to the *step* 1 but in the y direction, that is, to compress OE to OE'. The last step (*step* 3) is only to compress OF to OF' in the z direction. Let $OA = a$, $OB = b$, $OC = c$, $OD = d$, $OD' = d'$, $OE = e$, $OE' = e'$, $OF = f$, and $OF' = f'$. Transformation steps are described as follows.

In *step* 1, the original space (x, y, z) is transformed into the transitional space (x', y', z'). The region *1* (*ABCD*) in Fig. 2a is stretched into region *1* (*ABCD'*) in Fig. 2b. Similarly, regions *2*, *3* and *4* in Fig. 2a are compressed into the corresponding regions in Fig. 2b. For each region, the coordinate transformation equations can be described as follows.

$$\text{Region 1: } x' = \frac{a - d'}{a - d}x - \frac{a(d - d')}{b(d - a)}y - \frac{a(d - d')}{c(d - a)}z - \frac{a(d - d')}{d - a}, \quad y' = y, \quad z' = z; \quad (14)$$

$$\text{Region 2: } x' = \frac{d'''}{d}x, \quad y' = y, \quad z' = z; \quad (15)$$

$$\text{Region 3: } x' = \frac{d'}{d}x, \quad y' = y, \quad z' = z; \quad (16)$$

$$\text{Region 4: } x' = \frac{d'}{d}x, \quad y' = y, \quad z' = z. \quad (17)$$

In *step* 2, the transitional space (x', y', z') is transformed into(x'', y'', z''), and OE is compressed to OE' in the y direction. From Fig. 2c, it can be seen that

region *1* keeps unchanged; region *2* is stretched; regions *3* and *4* are relatively compressed. The corresponding mapping for each region can be expressed by the following equations.

$$\text{Region 1: } x'' = x', \quad y'' = y', \quad z'' = z'; \tag{18}$$

$$\text{Region 2: } x'' = x', \quad y'' = -\frac{b(e-e')}{d'(e-b)}x' + \frac{b-e'}{b-e}y' - \frac{b(e-e')}{c(e-b)}z' + \frac{b(e-e')}{e-b}, \quad z'' = z'; \tag{19}$$

$$\text{Region 3: } x'' = x', \quad y'' = \frac{e'}{e}y', \quad z'' = z'; \tag{20}$$

$$\text{Region 4: } x'' = x', \quad y'' = \frac{e'}{e}y', \quad z'' = z'. \tag{21}$$

In *step* 3, the transitional space (x'', y'', z'') is further mapped onto the transformed space (x''', y''', z'''), as shown in Figs. 2c–2d. The line segment OF is compressed into OF' in z direction, and then region *3* is stretched and region *4* is compressed. It should be noted that regions *1* and *2* experience no distortions during *step* 3. The transformation equations of the four regions can be written as

$$\text{Region 1: } x''' = x'', \quad y''' = y'', \quad z''' = z''; \tag{22}$$

$$\text{Region 2: } x''' = x'', \quad y''' = y'', \quad z''' = z''; \tag{23}$$

$$\text{Region 3: } x''' = x'', \quad y''' = y'', \quad z''' = -\frac{c(f-f')}{d'(f-c)}x'' - \frac{c(f-f')}{e'(f-c)}y'' + \frac{c-f'}{c-f}z'' + \frac{c(f-f')}{f-c}; \tag{24}$$

$$\text{Region 4: } x''' = x'', \quad y''' = y'', \quad z''' = \frac{f'}{f}z''. \tag{25}$$

Combing these three steps, the transformation equations from original space to the transformed space are summarized as follows.

$$\text{Region 1: } x''' = \frac{a-d'}{a-d}x - \frac{a(d-d')}{b(d-a)}y - \frac{a(d-d')}{c(d-a)}z + \frac{a(d-d')}{d-a}, \quad y''' = y, \quad z''' = z; \tag{26}$$

$$\text{Region 2: } x''' = \frac{d'}{d}x, \quad y''' = -\frac{b(e-e')}{d(e-b)}x + \frac{b-e'}{b-e}y - \frac{b(e-e')}{c(e-b)}z + \frac{b(e-e')}{e-b}, \quad z''' = z; \tag{27}$$

$$\text{Region 3: } x''' = \frac{d'}{d}x, \quad y''' = \frac{e'}{e}y, \quad z''' = -\frac{c(f-f')}{d(f-c)}x - \frac{c(f-f')}{e(f-c)}y + \frac{c-f'}{c-f}z + \frac{c(f-f')}{f-c}; \tag{28}$$

$$\text{Region 4: } x''' = \frac{d'}{d}x, \quad y''' = \frac{e'}{e}y, \quad z''' = \frac{f'}{f}z. \tag{29}$$

Finally, substituting Eqs. (26)–(29) into Eq. (1), the mass density tensor and bulk modulus of regions *1*, *2*, *3* and *4* in the first quadrant can be obtained.

$$\text{Region 1: } \frac{1}{\rho_1'} = \begin{bmatrix} (A^2 + B^2C^2 + B^2D^2)/A & -BC/A & -BD/A \\ -BC/A & 1/A & 0 \\ -BD/A & 0 & 1/A \end{bmatrix}\frac{1}{\rho}, \quad \kappa_1' = A\kappa; \tag{30}$$

$$\text{Region 2: } \frac{1}{\rho_2'} = \begin{bmatrix} M/E & -FG/E & 0 \\ -FG/E & (F^2G^2 + E^2 + F^2H^2)/(ME) & -FH/(ME) \\ 0 & -FH/(ME) & 1/(ME) \end{bmatrix}\frac{1}{\rho}, \quad \kappa_2' = ME\kappa; \tag{31}$$

$$\text{Region 3: } \frac{1}{\rho_3'} = \begin{bmatrix} M/(NI) & 0 & -JK/(NI) \\ 0 & N/(MI) & -JL/(MI) \\ -JK/(NI) & -JL/(MI) & (J^2K^2 + J^2L^2 + I^2)/(MNI) \end{bmatrix}\frac{1}{\rho}, \quad \kappa_3' = MNI\kappa; \tag{32}$$

$$\text{Region 4: } \frac{1}{\rho_4'} = \begin{bmatrix} M/(NR) & 0 & 0 \\ 0 & N/(MR) & 0 \\ 0 & 0 & R/(MN) \end{bmatrix}\frac{1}{\rho}, \quad \kappa_1' = MNR\kappa, \tag{33}$$

where $A = (a-d')/(a-d)$, $B = (d-d')/(d-a)$, $C = a/b$, $D = a/c$, $E = (b-e')/(b-e)$, $F = (e-e')/(e-b)$, $G = b/d$, $H = b/c$, $I = (c-f')/(c-f)$, $J = (f-f')/(f-c)$, $K = c/d$, $L = c/e$, $M = d'/d$, $N = e'/e$ and $R = f'/f$.

Similarly, material parameters of the remaining parts of the 3D acoustic concentrator can be obtained by means of axial symmetry. Obviously, the material parameters are also homogeneous and non-singular.

3. SIMULATION RESULTS AND DISCUSSIONS

In this section, we carry out full-wave simulations using the commercial finite element solver COMSOL Multiphysics to demonstrate the performance of the

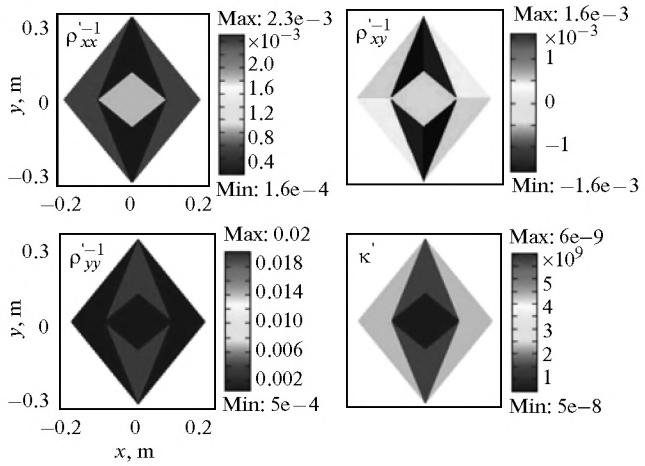

Fig. 3. Material parameter distributions for the 2D acoustic concentrator.

designed concentrators. Water is chosen as the background medium, and its mass density and bulk modulus are $\rho = 998$ kg/m^3 and $\kappa = 2.18 \times 10^9$ Pa.

3.1. 2D Acoustic Concentrator

For the 2D acoustic concentrator, the geometry parameters are arbitrarily chosen as $a = 0.15$ m, $b = 0.1$ m, $c = 0.2$ m, $d = 0.3$ m, $e = 0.25$ m, and $f = 0.1$ m. It should be noted that the diamond-shaped region being transformed can even be beyond the outer shell of the concentrator (i.e. $a > c$ and/or $e > d$), but in transformed space the transformed region should be strictly within the outer shell (i.e. $b < c$ and $f < d$), which is similar to the case of the electromagnetic concentrator [13, 28–32]. Figure 3 shows the material parameter distributions for the 2D acoustic concentrator in the transformed space. It is clear that the mass density tensor and bulk modulus are spatially invariant and symmetric, and there are no singular value. These properties are distinguished from the current acoustic concentrator case [27], and thus greatly enhance the reliability of the acoustic concentrator in practice. Although the required parameters are still anisotropic, they are adjustable by changing the geometry parameters of concentrator, and accessible from metamaterials [33–36].

Figure 4 shows the pressure field distributions in the vicinity of acoustic concentrator under the illumination of plane wave and cylindrical wave. Figures 4a and 4c display the pressure field distributions when 8 kHz acoustic plane wave with an amplitude of 1 Pa is incident from left to right and from top to bottom, respectively. Figure 4b shows the distribution of acoustic pressure field under cylindrical wave irradiation. The 8 kHz line source with a flow of 3e–7 W/m^2 in

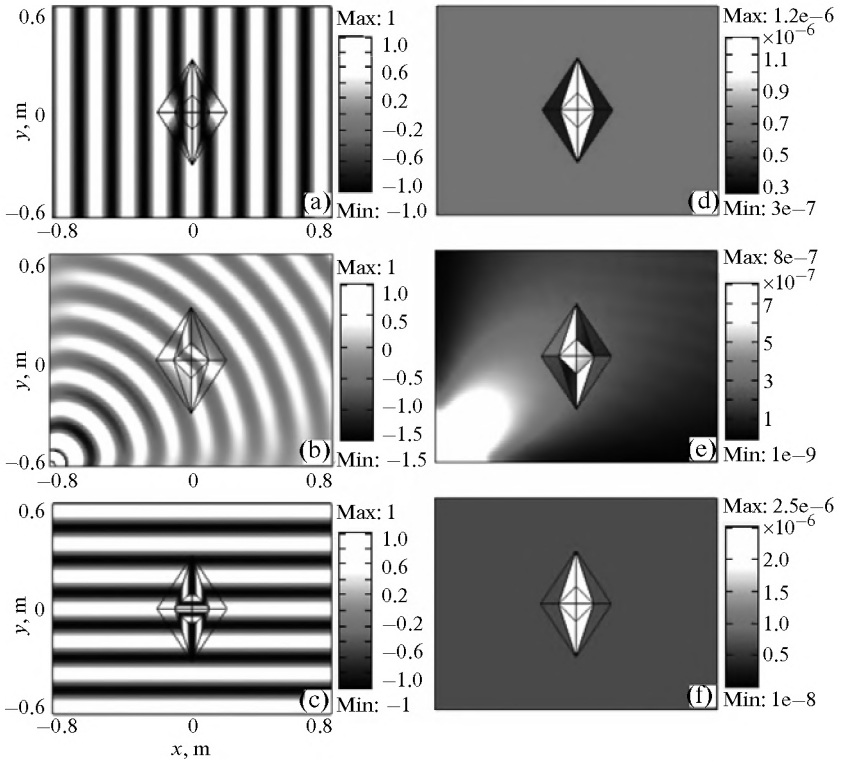

Fig. 4. The pressure field distributions in the vicinity of the 2D acoustic concentrator under the illuminations of plane wave and cylindrical wave. (a) The plane wave is incident from left to right, (b) the line source is located at (–0.8, –0.6 m), (c) the plane wave is incident from top to bottom, (d–f) are the corresponding acoustic intensity distributions of (a–c).

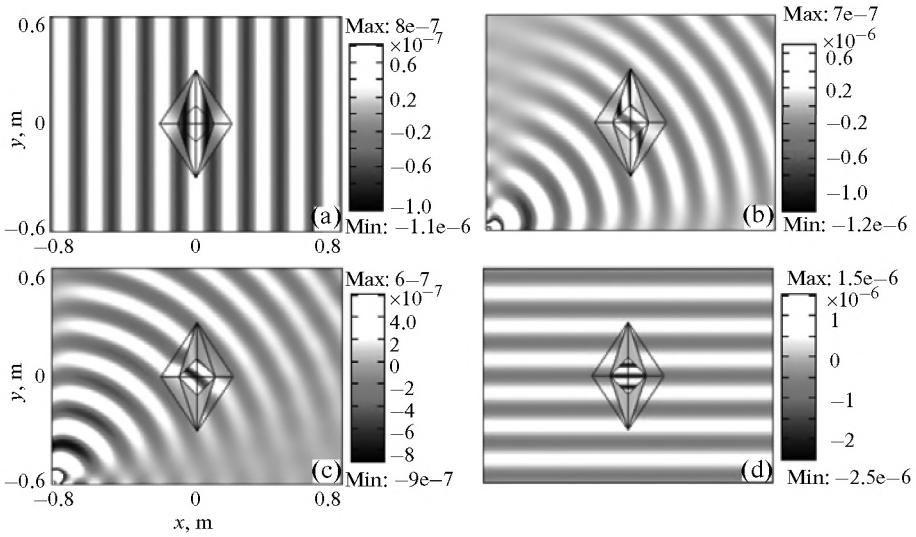

Fig. 5. x-Component of the local velocity (v_x) distributions in the vicinity of the concentrator when a plane wave is incident from left to right (a), and a line source is located at (−0.8, −0.6 m) (b). y-Component of the local velocity (v_y) distributions in the vicinity of the concentrator when a line source is located at (−0.8, −0.6 m) (c), and a plane wave is incident from top to bottom (d).

z direction is located at (−0.8, −0.6 m). It can be seen that the acoustic waves in three cases are perfectly focused by the concentrator into the compressive region. That is to say, the performance of the concentrator is independent on the direction of the incident wave and the shape of the wave front. Interestingly, the amplitude of the acoustic pressure field in the core of the concentrator is the same as that in free space. The phenomenon is caused by the design method of the concentrator which only compresses the space in the x and y directions, while keeps the z direction undistorted. In order to give a more convincing and clearer illustration for the performance of the concentrator, the distributions of normalized acoustic intensity corresponding to Figs. 4a–4c are shown in Figs. 4d–4f. As can be seen from Figs. 4d–4f, the acoustic intensity in the compressive region is strongly enhanced for all incident directions. Therefore, the effectiveness of the material parameters we develop are well verified.

The x and/or y components of the local velocity (v_x and/or v_y) are magnified since the space is compressed in x and y directions, and thus the acoustic intensity is enhanced in the compressive region of the concentrator. To confirm this point, the component of the local velocity distributions under the illuminations of plane wave and cylindrical wave are shown in Fig. 5. Since v_y is zero in the computational region when a plane wave is incident from left to right, it is not given here. The same reason for v_x when a plane wave impinges on the concentrator from top to bottom. In Fig. 5, it is clear that the components of the local velocity in compressive region of the concentrator are amplified with respect to that out of the device. Thus, the reason for the enhancement of acoustic intensity in the compressive region is validated.

3.2. 3D Acoustic Concentrator

The geometry parameters related to the shape and size of the 3D acoustic concentrator in the simulation are set to be $a = 0.4$ m, $b = 0.8$ m, $c = 0.2$ m, $d = 0.3$ m, $d' = 0.2$ m, $e = 0.6$ m, $e' = 0.4$ m, $f = 0.15$ m, and $f' = 0.1$ m. The simulation area is 2.5 × 2 × 1 m. In the whole computational domain, both the inner and outer boundaries of the concentrator are continuous boundary conditions. The outer boundary of the domain contains four PEC boundaries and two wave ports. A 5 kHz uniform plane wave with a pressure amplitude of 1 Pa is incident onto the acoustic concentrator from the $-x$ direction to the $+x$ direction.

Figures 6a and 6b show the pressure field distributions of the acoustic concentrator in 3D profile and 2D plane (xoy). The simulation results in xoz plane are not included herein for brevity. From Figs. 6a and 6b, we can observe that acoustic plane waves are focused into the compressive region, and they recovered the original propagation status when passing through the concentrator. To further investigate the performance of the acoustic concentrator, the corresponding acoustic intensity distributions of Figs. 6a and 6b are shown in Figs. 6c and 6d, respectively. It is obvious that acoustic intensity is greatly enhanced in the compressive region. Hence the perfect concentrating effect in 3D case is clearly demonstrated. Generally, much stronger enhancements can be achieved by diminishing the size of the compressive region through decreasing the ratio of $d'/d = e'/e = f'/f = \tau$. The acoustic intensity distributions along z axis at $x = 0$ and $y = 0$ with different values of τ are plotted in Fig. 7. It is seen that the acoustic intensity of the compressive region with $\tau = 1/5$ is about 3.8 times larger than that of the case with $\tau = 2/3$. The enhancement theoretically

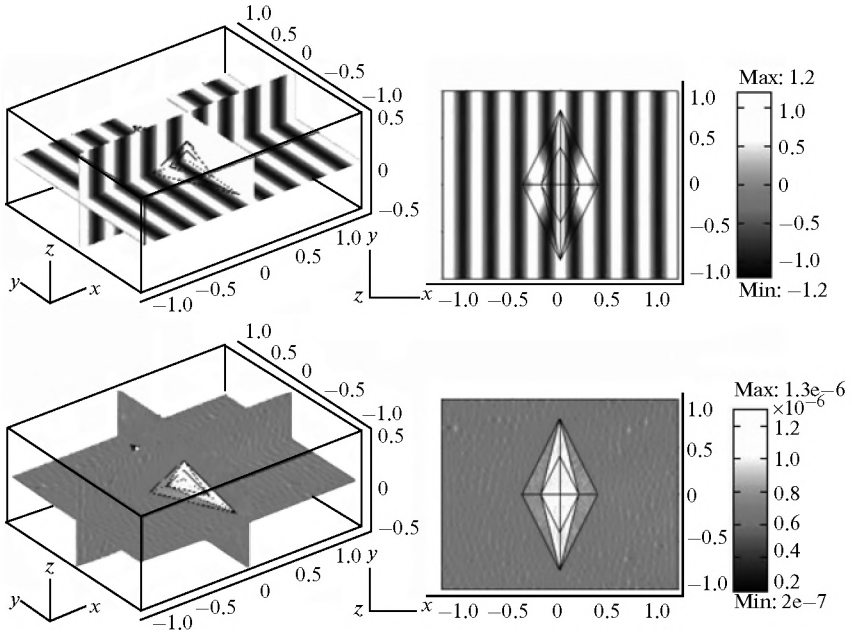

Fig. 6. The pressure field distributions in the vicinity of the 3D acoustic concentrator when the incident plane wave propagates along x axis, (a) 3D profile, (b) xoy plane, (c) and (d) are the corresponding acoustic intensity distributions of (a) and (b).

diverges to infinity as the volume of the compressive region goes to zero. The "step-like" pattern is believed to be induced by the numerical method due to discretization. It can be improved by fine mesh with the cost of memory consumption and computation time.

4. CONCLUSIONS

In this paper, both 2D and 3D diamond-shaped acoustic concentrators are proposed and designed based on the coordinate transformation method. The mass density tensor and bulk modulus are derived, and verified by full-wave simulation. The linear transformation avoids the singularity in the material parameters. Moreover, due to homogeneously stretching and compressing at the orthogonal directions during the transformation, the resulted material parameters are homogeneous. Numerical results show that performance of the concentrator is independent on the direction of incident wave and the shape of wave front, and the derived material parameters will greatly facilitate the practical fabrication of acoustic concentrator. The proposed design method can also be utilized for designing nonsingular homogeneous acoustic invisibility cloak, carpet cloak, superscatterer, etc.

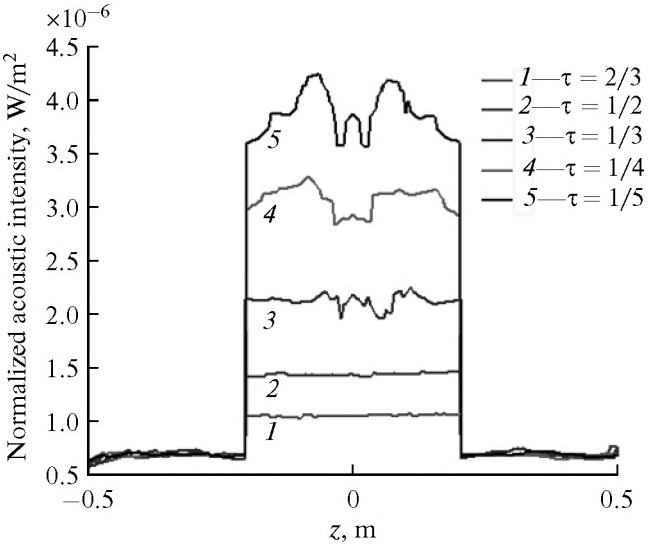

Fig. 7. Acoustic intensity distributions along z axis at $x = 0$ and $y = 0$ with different values of τ.

ACKNOWLEDGMENTS

This work was supported by the National Natural Science Foundation of China (grant no. 61161007), Scientific Research Fund Major Project of the Education Bureau of Yunnan Province (grant no. ZD2011003), the Natural Science Foundation of Yunnan Province (project no. 2011FB018), and the Scientific Research Foundation of Yunnan University (grant no. 2010YB025).

REFERENCES

1. J. B. Pendry, D. Schurig, and D. R. Smith, Science **312**, 1780 (2006).
2. U. Leonhardt, Science **312**, 1777 (2006).

3. S. A. Cummer, B. I. Popa, D. Schurig, and D. R. Smith, Phys. Rev. E: Statist., Nonlinear, Soft Matter Phys. **74**, 036621 (2006).
4. D. Schurig, J. J. Mock, B. J. Justice, et al., Science **314**, 977 (2006).
5. W. S. Cai, U. K. Chettiar, A.V. Kildishev, and V. M. Shavlaev, Nat. Photon **1** 224 (2007).
6. U. Leonhardt and T. Tyc, Science **323**, 110 (2008).
7. R. Liu, C. Ji, J. J. Mock, et al., Science **323**, 366 (2009).
8. H. Y. Chen, C. T. Chan, and P. Sheng, Nature Mater. **9**, 387 (2010).
9. W. X. Jiang, J. Y. Chin, and T. J. Cui, Materials Today **12** (12), 26 (2009).
10. D. H. Kwon and D. H. Werner, IEEE Antennas Propagation Mag. **52** (1), 24 (2010).
11. H. Y. Chen and C. T. Chan, Appl. Phys. Lett. **90**, 241105 (2007).
12. M. Rahm, S. A. Cummer, D. Schurig, et al., Phys. Rev. Lett. **100**, 063903 (2008).
13. J. J. Yang, M. Huang, C. F. Yang, et al., Opt. Express **17**, 19656 (2009).
14. W. Wang, L. Lin, X. F. Yang, et al., Opt. Express **16**, 8094 (2008).
15. J. J. Yang, M. Huang, C. F. Yang, and J. Yu, Eur. Phys. J. D: At., Molec., Opt., Plasma Phys. **61**, 731 (2011).
16. S. A. Cummer and D. Schurig, New J. Phys. **9**, 45 (2007).
17. H. Y. Chen and C. T. Chan, Appl. Phys. Lett. **91**, 183518 (2007).
18. J. J. Yang, M. Huang, C. F. Yang, et al., Comput. Mater. Sci. **49** (1), 9 (2010).
19. H. Y. Chen, J. Yang, J. Zi, and C. T. Chan, Europhys. Lett. **85**, 24004 (2009).
20. J. Han, Y. C. Fan, H. Q. Li, and Z. S. Wang, 2009. arXiv:0905.3422v1.
21. T. Yang, R. F. Cao, X. D. Luo, and H. R. Ma, Appl. Phys. A: Mater. Sci. Proces. **99**, 843 (2010).
22. C. Y. Ren, Z. H. Xiang, and Z. Z. Cen, Appl. Phys. **97**, 044101 (2010).
23. L. Y. Wu and L. W. Chen, J. Phys. D: Appl. Phys. **44**, 125402 (2011).
24. H. Y. Chen and C. T. Chan, J. Phys. D: Appl. Phys. **43**, 113001 (2010).
25. V. A. Grigor'ev and V. M. Kuz'kin, Acoust. Phys. **51**, 292 (2005).
26. A. L. Virovlyansky, A. Yu. Kazarova, and L. Y. Lyubavin, Acoust. Phys. **57**, 824 (2011).
27. J. J. Yang, M. Huang, C. F. Yang, and G. H. Cai, J. Vib. Acoust. **133**, 061016 (2011).
28. W. Li, J. G. Guan, and W. Wang, J. Phys. D: Appl. Phys. **44**, 125401.1 (2011).
29. M. Rahm, D. Schurig, D. A. Roberts, et al., Photon. Nanostruct. Fundam. Appl. **6** (1), 87 (2008).
30. L. Lin, W. Wang, C. L. Du, and X. G. Luo, Opt. Express **16**, 6809 (2008).
31. C. F. Yang, J. J. Yang, M. Huang, et al., J. Opt. Soc. Am. A **27**, 1994 (2010).
32. W. Wang, L. Lin, J. X. Ma, et al., Opt. Express **16**, 11431 (2008).
33. A. Sihvola, S. Tretyakov, and A. de Baas, J. Commun. Technol. Electron. **52**, 986 (2007).
34. V. A. Burov, K. V. Dmitriev, and S. N. Sergeev, Acoust. Phys. **55**, 298 (2009).
35. Y. I. Bobrovnitskii, Acoust. Phys. **58**, 30 (2012).
36. J. Christensen and F. J. G. de Abajo, Phys. Rev. Lett. **108**, 124301.1 (2012).